0266-3538(94)00029-8

IN SITU OBSERVATION OF THE SINGLE-FIBER FRAGMENTATION PROCESS IN METAL-MATRIX COMPOSITES BY ULTRASONIC IMAGING

M. C. Waterbury,[a] P. Karpur,[b] T. E. Matikas,[b] S. Krishnamurthy[a] & D. B. Miracle[c]

[a]Universal Energy Systems Inc., 4401 Dayton-Xenia Road, Dayton, Ohio 45432-1894, USA
[b]Research Institute, University of Dayton, 300 College Park Avenue, Dayton, Ohio 45469-0127, USA
[c]Materials Development Branch, Materials Directorate, Wright Laboratory, Wright-Patterson Air Force Base, Ohio 45433-7817, USA

Abstract

Single-fiber fragmentation tests with continuous silicon-carbide fibers in a Ti–6Al–4V alloy matrix have been conducted with in situ ultrasonic imaging to monitor the fragmentation process. Straining proceeded incrementally on a specially designed load frame with acoustic emission detection (AE) performed during each increment, and shear-wave back reflectivity (SBR) ultrasound images were acquired following each increment. Metallographic examination of the fragmented fiber was performed following the straining sequence by electropolishing and scanning electron microscopy. Good agreement was found between the fiber breaks imaged by ultrasound, the number of breaks detected by acoustic emissions, and the breaks observed by metallography.

Keywords: ultrasound, NDE, fragmentation, metal-matrix composite, acoustic emission

INTRODUCTION

The performance of ceramic-fiber-reinforced titanium-matrix and intermetallic-matrix composites is limited by reactions at the fiber/matrix interface which both degrade fiber strength and generate brittle reaction products in the matrix. Protective fiber coatings, such as the carbon-rich layers on SCS-6 fibers, reduce this damage but result in extremely poor interfacial adhesion. Optimization of the fiber/matrix interface properties in these composites has lagged behind other aspects of their development.

The single-fiber fragmentation test[1-3] has been widely used and studied in recent years as an indicator of approximate fiber/matrix interfacial adhesion. Application of this test has been limited, with some exceptions,[4-6] to transparent matrices because the resultant fiber fragments must be visually observed to be measured. Acoustic emission has been used to count fiber failure events and locate fiber breaks.[5] This method is complicated, however, by the interactions between the shear and longitudinal waves generated by fiber failures and the specimen geometry. Ultrasonic imaging has been used recently to image fiber fragments for composite systems with sufficiently large fiber diameters.[6,7]

Fragmentation testing has also been proposed[4,8,9] as a method for measuring fiber strengths in situ. This method has been experimentally verified[8] by counting the numbers of fiber failures occurring within given coupon strain increments during the early portions of the fragmentation process and applying an appropriate analytical treatment. Fiber strengths in titanium-matrix composites may be severely degraded during consolidation and service and may also be influenced by residual stresses and failures initiated within the brittle fiber/matrix reaction zone. In situ fiber strength information is therefore an important parameter for composite performance that is not accessible by other means.

The interpretation of fragmentation tests in ceramic fiber-reinforced metal and intermetallic matrices is particularly difficult because of the presence of multiple interfaces between the fiber, its coatings, and the matrix. The presence of several potential failure initiation sites and secondary fiber failure events further complicates the analysis, as does damage induced by specimen preparation. In situ non-destructive observation of single-fiber composites after each of several small strain increments can aid interpretation by providing more complete information than a single destructive observation after fiber fragmentation. High frequency (25 MHz) ultrasound imaging can perform such non-destructive observation[6,7] for systems with sufficiently large fiber diameters, such as the 142 μm silicon-carbide fibers used in this study. In addition to information on fiber break locations, the technique may provide useful

data on the interfacial debonding that occurs adjacent to the breaks.

The objective of this paper is to report on the use of combined non-destructive SBR ultrasound imaging and acoustic emission monitoring with an *in situ* micro-straining stage, and post-test scanning electron microscopy to better understand the process of single-fiber fragmentation in titanium-matrix composites.

EXPERIMENTAL

Sheets of Ti–6Al–4V 1·27 mm thick were used as the matrix material. Textron SCS-6 silicon carbide fibers 142 μm in diameter were used for the reinforcements. Fibers were aligned by placing them in a fiber-retention groove that was machined with a specially constructed shaping apparatus in one titanium preform plate, as shown in Fig. 1. Specimens were fabricated by hot pressing at 954°C/10 MPa for 75 min followed by cooling at 10°C/min.

Specimens were strained with a specially constructed *in situ* straining stage which was designed for low frame compliance and low background noise for acoustic emission work. A simple, compact design was used so that ultrasound imaging could be performed without removing the specimen from the straining stage and releasing the specimen strain. Straining proceeded in nominal increments of 0·75%, with the acoustic emission recorded during each strain increment. The straining stage with the loaded sample was then placed in a water tank, and ultasonic imaging was performed after each strain increment. The stage is shown in the imaging tank with the acoustic transducer in position in Fig. 2.

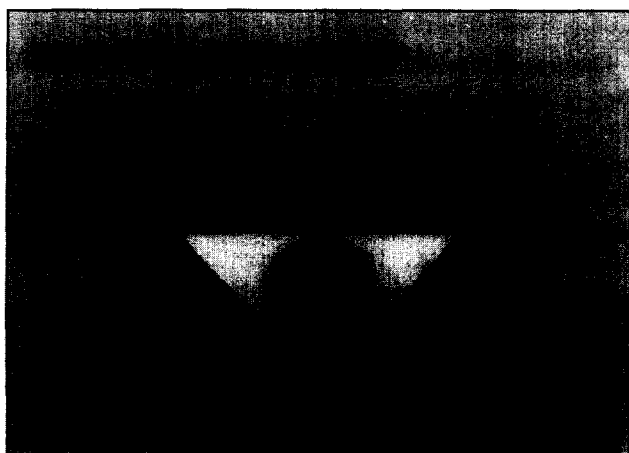A 25 MHz focused transducer (6·4 mm diameter,

Fig. 1. Schematic diagram of silicon-carbide fiber in a fiber retention and protection groove machined into a titanium-alloy preform plate. The fiber is protected from damage by point loading during consolidation and is accurately aligned and positioned.
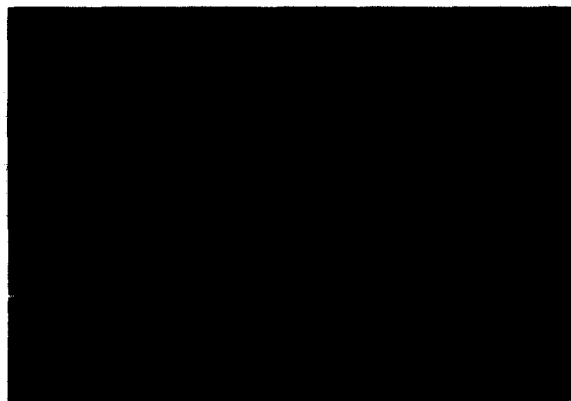

Fig. 2. Single-fiber fragmentation specimen in microstraining stage with the ultrasonic sensor in position, aligned at an angle of 24°. Acoustic emission sensors, normally attached at specimen ends, are not included for clarity.

12·7 mm focus) was used in the pulse-echo mode for the imaging of the embedded fiber. The shear-wave back reflectivity (SBR) technique was used wherein the ultrasonic wave front was incident on the composite at an angle of 24° (which is between the first and the second critical angles). As a result, vertically polarized shear waves were incident on the interface between the fiber and the matrix. Back-reflected ultrasound waves were gated for imaging. Since the wave front was incident at an angle, the received signal was either low amplitude due to back-scattering from the material texture or a very strong amplitude due to the back-reflection from the cylindrical fiber. As a result, the dynamic range of the image of the fiber was excellent. Also, the wave front was slightly defocused (−1·52 mm) in the fiber interface. The reasoning for the defocus can be explained using acoustic interference and can be found in the literature.[7]

Acoustic emission data were collected with a Physical Acoustics Locan AT acoustic emission data acquisition system with 8 mm diameter broadband transducers and 40 Db preamplifiers with 100–400 KHz bandpass filters.

Previous work (Krishnamurthy, S. & Roman, I., unpublished) has shown that fiber damage is introduced during metallographic sectioning by mechanical means, and the smallest fiber pieces, associated with secondary fiber fractures generated during the fragmentation test, are typically lost. Therefore, following straining, specimens were electropolished to expose the fiber fragments for observation. Polishing was performed in a solution consisting of 500 ml methanol, 300 ml ethylene glycol monobutyl ether, and 36 ml of a 60% aqueous solution of perchloric acid. The solution was maintained at −40°C and was agitated by argon bubbling. The specimen was held approximately 1 cm from the electrode and polishing proceeded at a 13 V
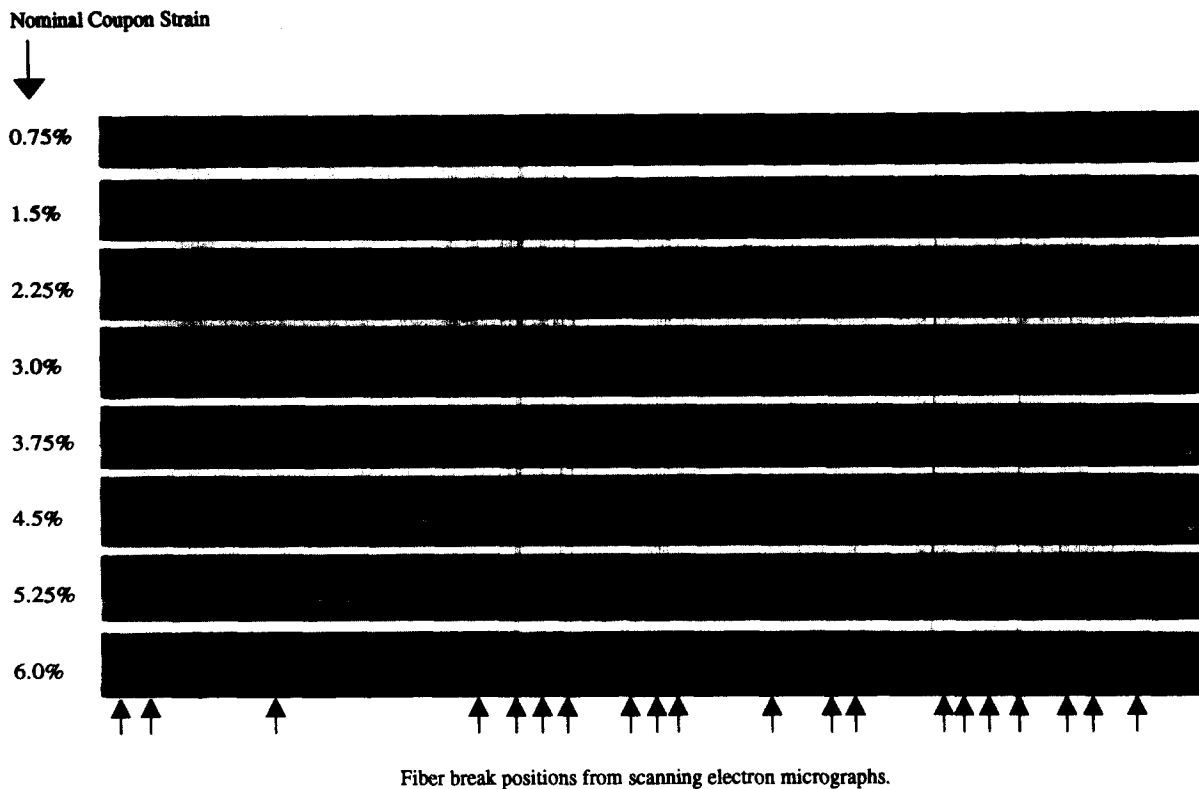
Fig. 3. SBR ultrasound images of single-fiber fragmentation specimen at increasing strain levels (top to bottom). Positions of fiber breaks observed by scanning electron microscopy are shown at the bottom.

potential until initial fiber exposure. Acid-resistant lacquer was then applied to exposed areas followed by subsequent electropolishing until the fiber was exposed along the entire specimen gage section.

Scanning electron microscopy of the electropolished samples was performed with a field emission scanning electron microscope (SEM). Digital images produced with this system were downloaded to a computer and assembled with a graphics program into a single, contiguous, high-resolution image of the entire fragmented fiber, some 23 000 pixels in length. Fiber breaks were identified in this image and in other higher magnification images, and compared with the images obtained by ultrasonic imaging.

RESULTS AND DISCUSSION

A single-fiber fragmentation specimen imaged by reflected ultrasound is shown in Fig. 3, with increasing coupon strain levels moving from top to bottom in nominal strain increments of 0·75%. The positions of fiber breaks observed by SEM are plotted as arrows at the bottom of the figure. Interpretation of the SBR ultrasound images must be performed with a recognition of the resolution limits of the technique in relation to the fiber size. Figure 4 shows a scanning electron micrograph of a fiber break, an SBR ultrasound image and the wavelength of the 25 MHz
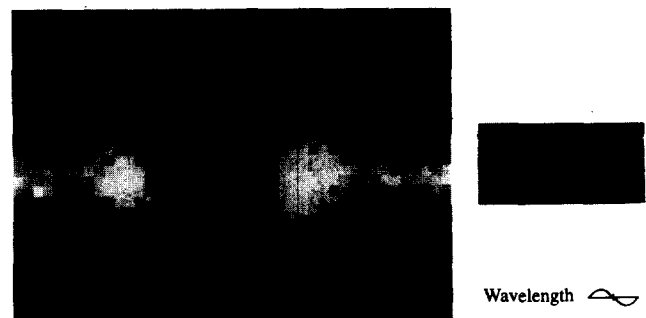

Fig. 4. SBR ultrasound image of fiber break along with SEM image of a break shown at the same scale. The resolution of the technique is of a comparable size as the features being imaged, complicating interpretation. The wavelength of the interrogation frequency in this material is shown to the right.

interrogation sound (128 μm) all at the same scale. Since the fiber diameter and the wavelength are approximately the same size, the SBR ultrasound data does not provide a simple, resolved image of the fiber and breaks in it, but only an indication of regions where there is sonic interference due to fiber breaks.[7]

Before fragmentation begins, the fiber/matrix interface uniformly reflects the ultrasound, producing the homogeneous band in the topmost image. The first fiber breaks produce clear patterns consisting of pairs

of dark regions where the sound reflecting from the new surfaces created by the fiber fracture destructively interferes, with a central bright region where constructive interference occurs.[7] When the spacing between fiber breaks is large, the pattern of constructive and destructive interference is unambiguous and easy to interpret in terms of break locations. With smaller break-to-break spacing at the end of the test, however, the observed ultrasound interference patterns may be the result of more than one possible fiber-break arrangement and interpretation becomes more difficult. The images of fiber breaks at prior coupon strain levels may be consulted in this case to determine the actual fiber break pattern.

The locations of the breaks observed by scanning electron microscopy, indicated by arrows at the bottom of Fig. 3, may be seen to correlate well with the features imaged by ultrasound. In a few cases, as near the left side of the figure, SBR ultrasound image features indicate the presence of a fiber break that is not visible under the SEM, but is apparently concealed by the reaction zone, which is not removed by electropolishing and is contiguous in these regions of the fiber. This interpretation is supported by the identification of other previously concealed fiber breaks by additional polishing. Changes in the polishing solution to allow it to attack the reaction zone and completely expose the fiber are under investigation.

Upon each fiber failure in a fragmentation specimen, elastic strain in the adjacent fiber fragments is relaxed by the retraction of the broken fiber ends, opening one or more cracks in the fiber. Simultaneously, the load formerly borne by the fiber is rapidly transferred through the fiber/matrix interfaces on either side of the fiber break to the adjacent matrix material. The shock wave produced by the failing fiber and the subsequent load redistribution, may initiate mode II interfacial cracks, mode I matrix cracks, or additional fiber fractures. No evidence of relaxation by mode I matrix cracks has been observed in the current study, although a shattered fiber morphology associated with fiber fragmentation is typically observed. As the strain in the fragmentation specimen is increased during subsequent strain increments, the interfacial cracks may propagate, and fretting damage and changes in acoustic reflectivity may occur.

Figure 5 shows a close-up of the ultrasonic reflection from a fiber break and the adjacent fiber fragments after additional strain increments. A change in reflectivity can be seen, beginning near the breaks and extending further away after additional strain increments, as indicated by the arrows on the figure. The causes of this change in reflectivity are unclear and are under investigation. In some cases, interference patterns generated between ultrasound waves
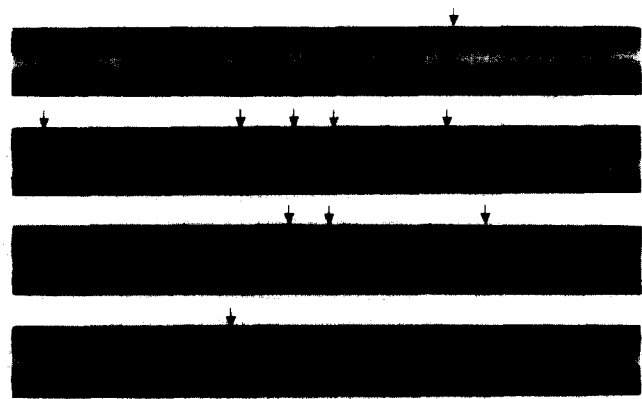

Fig. 5. Details of SBR ultrasound image of a fiber break shown at increasing strains. Changes in ultrasonic reflectivity adjacent to the break, indicated by arrows, may correspond to changes in the interface condition due to fiber/matrix debonding.

reflected by the fiber break and new, adjacent breaks produce a region of varying reflected ultrasound intensity that contrasts with the uniform intensity associated with intact, bonded fibers. Reflectivity changes may indicate that a mode II interfacial crack has initiated and propagated between the fiber and matrix near the break. The ability to observe fiber debonding by this method would provide a tool that is analogous to the use of optical birefringence patterns to assess failure modes in transparent polymer matrix fragmentation testing.[10,11] Additional studies are underway to determine the origins of these SBR ultrasound features.

The approximate positions of fiber breaks detected by acoustic emissions are shown in Fig. 6. Each strain increment is plotted separately with increasing strain from top to bottom, corresponding to the SBR ultrasound plots produced after the increment shown
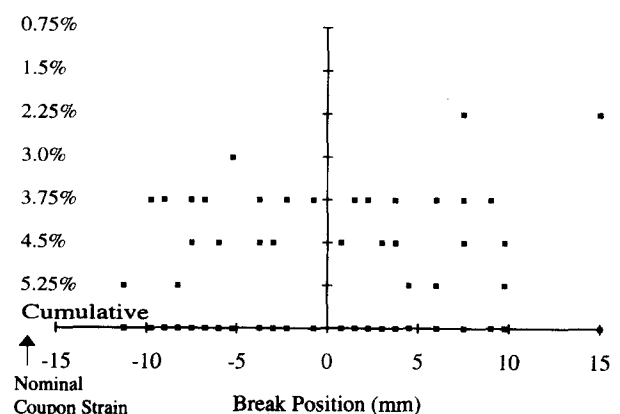

Fig. 6. Approximate positions of fiber breaks during each strain increment measured by acoustic emission time-of-flight method. Strain increments correspond to the SBR ultrasound images produced after each increment shown in Fig. 3. The cumulative positions of breaks are plotted at the bottom.
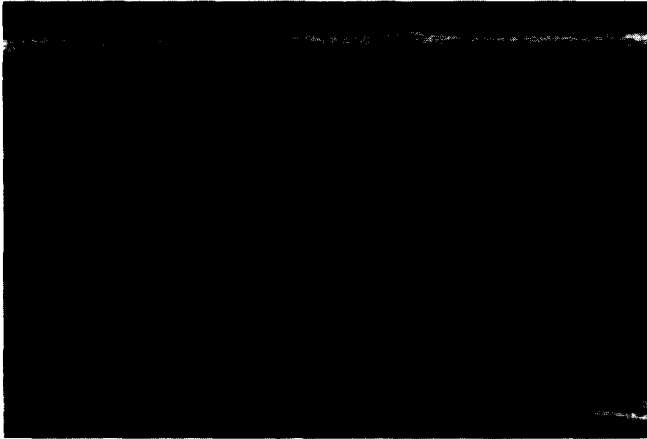
Fig. 7. SEM of the fiber fracture exposed by electropolishing. Four or five closely spaced breaks can be seen in the fiber through the gap in the reaction zone. Extensive reaction zone cracking can be seen, with crack spacings of approximately 30 μm (1/4–1/5 fiber diameter).

Fig. 8. SEM of fiber fracture exposed by electropolishing. Two or three closely-spaced fractures can be seen forming a V with angles from 90° to 70° from the fiber axis. The layer coating the fiber at the top and bottom is the reaction zone, shown by electron microprobe to contain titanium.
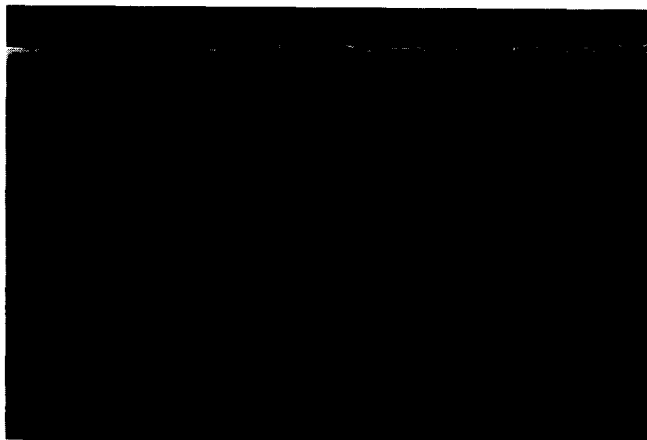

Fig. 9. SEM of fiber fracture exposed by electropolishing. Another common crack morphology, with multiple, closely spaced fracture surfaces fanned out from the center of the fiber. The fiber is mostly concealed by the outer surface of the reaction zone in this view.

in Fig. 3. The accuracy of determination of break locations by acoustic emission with the acoustic emission stystem used in this study is limited to approximately ±4 mm, limiting the inferences which may be drawn.

The fiber fracture morphologies were investigated by producing scanning electron micrographs of each visible fiber break after exposure by electropolishing, e.g. Figs 7–9. Fiber breaks did not generally consist of single fracture surfaces, but comprised a fractured zone, with two to five closely spaced fractures. These fractures appeared along a length of fiber 1/4 to 1/2 fiber diameters. It is believed that this morphology is generated by an initial tensile fiber failure, followed by additional damage produced by the fiber ends being driven back together in compression by a combination of the reflected elastic shock wave and the CTE mismatch forces. Exposure of the fiber by electropolishing was found to reveal the fracture morphology without the disruption of the fiber fragments that occurred during mechanical polishing.

Also evident from the SEM micrographs was the brittle reaction zone coating the fiber. Exposure of this reaction zone by electropolishing allows a non-uniform relaxation of CTE mismatch stresses, causing the exposed portion of the reaction zone to break and retract from the fiber, as seen in Figs 7 and 8.

CONCLUSIONS

The process of single-fiber fragmentation is silicon-carbide fiber reinforced Ti–6Al–4V matrix composites has been observed *in situ* by both shear-wave back-reflectivity ultrasound imaging and acoustic emission monitoring techniques and post-test by SEM observation of fibers exposed by electropolishing. Fiber breaks observed by SBR ultrasonic imaging correlated well with the numbers of breaks indicated by acoustic emission data and the positions and numbers observed by scanning electron microscopy. Well-separated fiber fractures may be clearly distinguished by SBR ultrasound imaging, while more closely spaced fractures produce interference between breaks which makes interpretation more difficult.

It has been shown in this paper that the multi-mode monitoring of fiber fragmentation provides more complete information about the fiber fragmentation process and final specimen state than does either technique in isolation.

F33615-89-C-5612 (P. Karpur), F33615-92-C-5663 (M. Waterbury and S. Krishnamurthy).

REFERENCES

1. Kelley, A. & Tyson, W. R., Tensile properties of fiber-reinforced metals: copper/tungsten and copper/molybdenum. *J. Mech. Phy. Solids*, **13** (1965) 329–50.
2. Fraser, W. A., Ancker, F. H., DiBenedetto, A. T. & Elbirli, B., Evaluation of surface treatments for fibers in composite materials. *Polymer Composites*, **4**(4) (1983) 238–48.
3. Drzal, L. T., Rich, M. J., Camping, J. P. & Park, W. J., A single filament technique for determining interfacial shear strength and failure mode in composite materials. In *Proceedings of 1980 Conference, Reinforced Plastics and Composites Institute*, SPI, Paper 20C, 1980(B).
4. Netravali, A. N., Topoleski, L. T. T., Sachse, W. H. & Phoenix, S. L., An acoustic emission technique for measuring fiber fragment length distributions in the single-fiber-composite test. *Composites Science and Technology*, **35** (1989) 13–29.
5. Waterbury, M. C., Nylon 6,6 Fragmentation Testing. In The Influence of Processing, Chemistry, and Interphase Microstructure on the Adhesion of Carbon Fibers to Thermoset and Thermoplastic Matrices. Dissertation, Michigan State University, 1991, pp. 201–2.
6. Karpur, P., Matikas, T., Krishnamurthy, S. & Ashbaugh, N., Ultrasound for fiber fragmentation size determination to characterize load transfer behavior of matrix-fiber interface in metal matrix composites. *Review of Progess in Quantitative NDE*, **12B** (1992) 1507–13.
7. Karpur, P., Matikas, T. E. & Krishnamurthy, S., Matrix-fiber interface characterization in metal matrix composites using ultrasonic imaging of fiber fragmentation. *American Society for Composites*, Pennsylvania State University, University Park, PA, 1992, pp. 420–9.
8. Waterbury, M. C. & Drzal, L. T., On the determination of fiber strengths by in situ fiber strength testing. *J. of Composites Technology & Research*, **13**(1) (Spring 1991) 22–8.
9. Curtin, W. A., Exact theory of fibre fragmentation in a single-filament composite. *J. of Materials Science*, **26** (1991) 5239–53.
10. Herrera-Franco, P. J., Rao, V. & Drzal, L. T., Bond strength measurement in composites—analysis of experimental techniques. *Comp. Engng*, **2** (1992) 31–45.
11. Waterbury, M. C., The influence of processing, chemistry, and interphase microstructure on the adhesion of carbon fibres to thermoset and thermoplastic matrices. Dissertation, Michigan State University, 1991, pp. 31–42.